

# GROMACS Stochastic Dynamics and BAOAB are equivalent configurational sampling algorithms

Stefanie Kieninger and Bettina G. Keller<sup>a)</sup>

*Department of Biology, Chemistry, Pharmacy, Freie Universität Berlin,  
Arnimallee 22, D-14195 Berlin, Germany*

(Dated: 6 April 2022)

Two of the most widely used Langevin integrators for molecular dynamics simulations are the GROMACS Stochastic Dynamics (GSD) integrator and the splitting method BAOAB. We show that the GROMACS Stochastic Dynamics integrator is equal to the less frequently used splitting method BAOA. It immediately follows that GSD and BAOAB sample the same configurations and have the same high configurational accuracy. Our numerical results indicate that GSD/BAOA has higher kinetic accuracy than BAOAB.

---

<sup>a)</sup>bettina.keller@fu-berlin.de

## I. INTRODUCTION

Langevin dynamics is an effective way to thermostat molecular dynamics (MD) simulations and to ensure that the simulations sample the canonical ensemble<sup>1</sup>. Two of the most widely used Langevin integrators are the GROMACS Stochastic Dynamics integrator (GSD)<sup>2</sup> and the BAOAB integrator<sup>3,4</sup>.

The GSD integrator is derived by extending the leap frog algorithm for deterministic dynamics by an impulsive application of friction. The algorithm exhibits first-order kinetics in the temperature relaxation and faithfully reproduces diffusion constants for a wide range of collision rates<sup>2</sup>. The algorithm has been implemented as the standard Langevin integrator in GROMACS<sup>5</sup> and is widely used in atomistic simulations<sup>6–8</sup>, coarse-grained simulations<sup>9–12</sup>, and dissipative particle simulations<sup>13,14</sup>. Besides its application within GROMACS, GSD has also been implemented and used in multiple other studies<sup>14–18</sup>.

The BAOAB integrator is based on splitting the vector field in the Langevin equation of motion into parts labelled A, B and O, and integrating these parts separately. The name BAOAB encodes the sequence of the integration steps. BAOAB has been implemented in OpenMMTools<sup>19,20</sup> for the MD package OpenMM<sup>21</sup> and is used frequently in atomistic MD simulations<sup>22,23</sup>. The method has been a starting point for the development of integration schemes for dynamics beyond classical MD, such as nonequilibrium MD<sup>24</sup>, generalized Langevin dynamics<sup>25–27</sup>, ab-initio path-integral MD<sup>28,29</sup>, and multi-timestep MD<sup>30,31</sup>. For any Langevin integrator, a systematic error in the sampled configurational Boltzmann density arises with increasing timestep. This error has been shown to be particularly small in BAOAB<sup>3,4,20,24,32</sup>. Thus, BAOAB can be operated at large timesteps - at least if the goal of the simulation is to sample the configurational Boltzmann density. For simulations of water, numerical stability up to timesteps of 6 to 9 fs have been reported<sup>20,33</sup>.

These two mainstay algorithms for MD simulations have so far been treated as separate integrators in the literature. Here, we argue that GSD and BAOAB sample the same configurations and similar momenta. For this, we show that the GSD equations can be rearranged to yield the BAOA integrator<sup>34</sup>. As has been noted previously, BAOA and BAOAB are closely related<sup>3,35,36</sup>: they sample the same positions and only differ by a shift of  $\frac{\Delta t}{2}$  in the momenta. We show that this similarity also extends to GSD.

## II. THEORY

### A. Langevin dynamics

Consider a particle with mass  $m$  that moves in a one-dimensional position space  $q \in \mathbb{R}$  according to underdamped Langevin dynamics

$$\begin{aligned}\dot{q} &= \frac{p}{m} \\ \dot{p} &= -\nabla_q V(q) - \xi p + \sqrt{2\xi k_B T m} \eta(t),\end{aligned}\tag{1}$$

where  $V(q)$  is the potential energy function at position  $q$ ,  $\nabla_q = \partial/\partial q$  denotes the gradient with respect to the position coordinate,  $\xi$  is a collision or friction rate (in units of  $\text{s}^{-1}$ ),  $T$  is the temperature and  $k_B$  is the Boltzmann constant.  $\eta \in \mathbb{R}$  is an uncorrelated Gaussian white noise with unit variance centered at zero  $\langle \eta(t)\eta(t') \rangle = \delta(t - t')$ , where  $\delta(t - t')$  is the Dirac delta-function. We use the dot-notation for derivatives with respect to time:  $\dot{q} = \partial q / \partial t$ .  $\omega(t) = (q(t), p(t)) \in \Omega \subset \mathbb{R}^2$  denotes the state of the system at time  $t$ , which consists of positions  $q(t)$  and conjugated momenta  $p(t) = m\dot{q}(t)$ .  $\Omega$  is called state space or phase space of the system.

A Langevin integrator  $I$  is a numerical integration scheme that solves eq. 1. It produces a time-discretized approximation  $\omega^I$  of a continuous trajectory  $\omega(t)$

$$\omega(t) \approx \omega^I = (\omega_1^I, \omega_2^I, \dots, \omega_n^I | \omega_0),\tag{2}$$

where  $\omega(t)$  denote an exact solution of eq. 1. The notation emphasises that the programme needs the initial state of the system  $\omega_0 = (q_0, p_0)$  as an input (initial condition).  $n$  is the number of integration timesteps  $\Delta t$ . We will denote the index of the integration timestep by  $k$ , such that  $\omega(t = k\Delta t) \approx \omega_k^I$ , and analogously  $q(t = k\Delta t) \approx q_k^I$  and  $p(t = k\Delta t) \approx p_k^I$ . Each of the Langevin integrators discussed here uses a single random number  $\eta_k$  of per integration step (and degree of freedom). Thus, given an initial state  $\omega_0$ , the timestep  $\Delta t$ , a potential energy function  $V(q)$  and a random number sequence  $\boldsymbol{\eta} = (\eta_1, \eta_2, \dots, \eta_n)$ , the trajectory  $\omega^I$  is defined unambiguously for a Langevin integrator  $I$ . However, with the same parameters different Langevin integrators yield slightly different trajectories, e.g.  $\omega^{\text{BAOAB}} \neq \omega^{\text{ABOBA}}$ . These differences determine the different numerical accuracies of Langevin integrators.

## B. GSD equals BAOA

We show that the GSD integrator is equal to a BAOA splitting algorithm. In Ref. 2, the GSD integrator is reported with the following equations

$$p = p_{k-\frac{1}{2}} - \nabla V(q_k) \Delta t \quad (3a)$$

$$\Delta p = -fp + \sqrt{f(2-f)mk_BT}\eta_k \quad (3b)$$

$$q_{k+1} = q_k + \left( \frac{p}{m} + \frac{1}{2} \frac{\Delta p}{m} \right) \Delta t \quad (3c)$$

$$p_{k+\frac{1}{2}} = p + \Delta p, \quad (3d)$$

where we made the following changes in the notation to be consistent with the notation in this contribution:  $h \rightarrow \Delta t$ ,  $a = F(t)/m \rightarrow -\frac{\nabla V(x(t))}{m}$ , and  $\xi \rightarrow \eta$ . We also denoted positions by  $q$  instead of  $x$ , and converted velocities into momenta:  $v = p/m$ . Finally, we multiplied eqs. 3a, 3b and 3d by  $m$  to obtain the algorithm in terms of the momenta. We changed time  $t$  into an iteration index  $k$ .

At the beginning of the integration step, position  $q_k$ , energy gradient  $-\nabla V(q_k)$ , and momentum  $p_{k-\frac{1}{2}}$  are known. Because the algorithm is an extension of the deterministic leap frog algorithm, the momenta generated in each iteration of the integrator are assigned to half timesteps  $k + \frac{1}{2}$ . In Ref. 2 the factor  $f$  is initially a user-defined parameter, but is later related to the friction coefficient  $\xi$  by

$$\xi = -\frac{1}{\Delta t} \ln(1-f) \Leftrightarrow f = 1 - e^{-\xi \Delta t} \quad (4)$$

(eq. 19 in Ref. 2), and thus

$$f(2-f) = (1 - e^{-\xi \Delta t}) \cdot (1 + e^{-\xi \Delta t}) = (1 - e^{-2\xi \Delta t}) . \quad (5)$$

Inserting eqs. 4 and 5 into eq. 3b yields

$$\Delta p = -p + e^{-\xi \Delta t} p + \sqrt{(1 - e^{-2\xi \Delta t}) mk_BT} \eta_k . \quad (6a)$$

Then eq. 3d reduces to

$$p_{k+\frac{1}{2}} = +e^{-\xi \Delta t} p + \sqrt{(1 - e^{-2\xi \Delta t}) mk_BT} \eta_k . \quad (7)$$

That is, eq. 3d can be expressed in terms of only  $p$ , and the intermediate calculation of  $\Delta p$  in eq. 6a can be omitted for the update of the momenta.

The position update in eq. 3c is a combination of two half-steps<sup>2</sup>: one after the first update of the momenta,  $p_{k-\frac{1}{2}} \rightarrow p$ , and one after the second update of the momenta  $p \rightarrow p_{k+\frac{1}{2}}$ :

$$\begin{aligned} q_{k+1} &= q_k + \left( \frac{p}{m} + \frac{1}{2} \frac{\Delta p}{m} \right) \Delta t \\ &= q_k + \frac{p}{m} \frac{\Delta t}{2} + \left( \frac{p}{m} + \frac{\Delta p}{m} \right) \frac{\Delta t}{2}, \end{aligned} \quad (8)$$

where the equations for the two half-steps are

$$q_{k+\frac{1}{2}} = q_k + p \frac{\Delta t}{2m} \quad (9a)$$

$$q_{k+1} = q_{k+\frac{1}{2}} + p_{k+\frac{1}{2}} \frac{\Delta t}{2m}. \quad (9b)$$

Combining the reformulated momentum update (eq. 7) and the two-step position update (eq. 9a and 9a) yields the BAOA method

$$p_k = p_{k-\frac{1}{2}} - \nabla V(q_k) \Delta t \quad (10a)$$

$$q_{k+\frac{1}{2}} = q_k + p_k \frac{\Delta t}{2m} \quad (10b)$$

$$p_{k+\frac{1}{2}} = +e^{-\xi \Delta t} p_k + \sqrt{(1 - e^{-2\xi \Delta t}) m k_B T} \eta_k \quad (10c)$$

$$q_{k+1} = q_{k+\frac{1}{2}} + p_{k+\frac{1}{2}} \frac{\Delta t}{2m}. \quad (10d)$$

Following the nomenclature in Refs. 3 and 4, eq. 10a is a *B*-step which updates the momenta according to the (deterministic) drift force, eqs. 10b and 10d are two *A'*-half-steps which update the positions according to the current momenta, and eq. 10c is an *O*-step which updates the momenta according to the stochastic force. Note that the *B*- and *O*-step use the full timestep  $\Delta t$ , while the *A'*-update has been split into two half-steps, each with  $\frac{\Delta t}{2}$ . We denote half-steps by '.

Since, eqs. 3a-3d and eqs. 10a-10d can be interconverted, the trajectories produced by these two algorithms for a given random number sequence  $\boldsymbol{\eta}$  must be identical:  $\boldsymbol{\omega}^{\text{GSD}} = \boldsymbol{\omega}^{\text{BAOA}}$ . This is the main result of this contribution.

### C. BAOA and BAOAB

We sketch the proof that BAOA<sup>34</sup> is equivalent to BAOAB<sup>3,4,24,32</sup>. A similar argument can be made based on the propagators of the two algorithms<sup>3</sup>. The BAOA algorithm iterates the

following substeps:  $BA'OA'; BA'OA'; BA'OA'; \dots$ , where half-steps with  $\frac{\Delta t}{2}$  are denoted by ' and semicolons show the end point of an integration cycle. A full  $B$ -step can be split into two consecutive  $B'$ -half-steps, which yields the following sequence of substeps:  $B'B'A'OA'; B'B'A'OA'; B'B'A'OA'; \dots$ . Since the algorithm is iterated, the choice of the endpoint of an integration cycle is somewhat arbitrary. One could denote the same sequence of steps as:  $B'; B'A'OA'B'; B'A'OA'B'; B'A'OA' \dots$ . This is the BAOAB algorithm. (See SI section 1 for the algorithm and SI Fig. 1 for a side-by-side comparison of BAOAB and BAOA.)

There are two differences between the BAOA and the BAOAB algorithm. First, the initial state of the iteration differs by a  $B'$ -half-step. To obtain identical intermediate results for BAOA and BAOAB for a given random number sequence  $\boldsymbol{\eta}$ , the initial momentum for BAOAB needs to be adjusted by a  $B'$ -half-step

$$p_0^{\text{BAOAB}} = p_0^{\text{BAOA}} - \frac{\Delta t}{2} \nabla V(q_0) \quad (11)$$

Second, the momenta, that are written to disc at the end point of an iteration, differ by a half-step  $B'$ . In summary, (with adjusted initial momenta) GSD, BAOA and BAOAB write identical position trajectories to disc, but the momentum trajectory of BAOAB differs slightly from the GSD/BAOA momentum trajectory.

### III. NUMERICAL RESULTS

#### A. Example trajectories

To verify that GSD, BAOA and BAOAB yield the same position trajectories, we calculated example trajectories with these three algorithms. Additionally we included ABOBA<sup>3,4</sup> in the comparison. (See SI section 1 for the algorithm.)

The trajectories were simulated in a one-dimensional tilted double well potential  $V(q) = (q^2 - 1)^2 + q$ . To be able to compare the integrators, we generated a sequence of 300 normally distributed random numbers  $\boldsymbol{\eta}$ , and used this  $\boldsymbol{\eta}$  for the integration with each of the integrators at  $\Delta t = 0.25$ . The initial conditions were  $q_0 = -0.5$  and  $p_0 = 1$  for all integrators except BAOAB, for which the initial momentum was adjusted according to eq. 11. (See SI section 2 for all simulation details.)

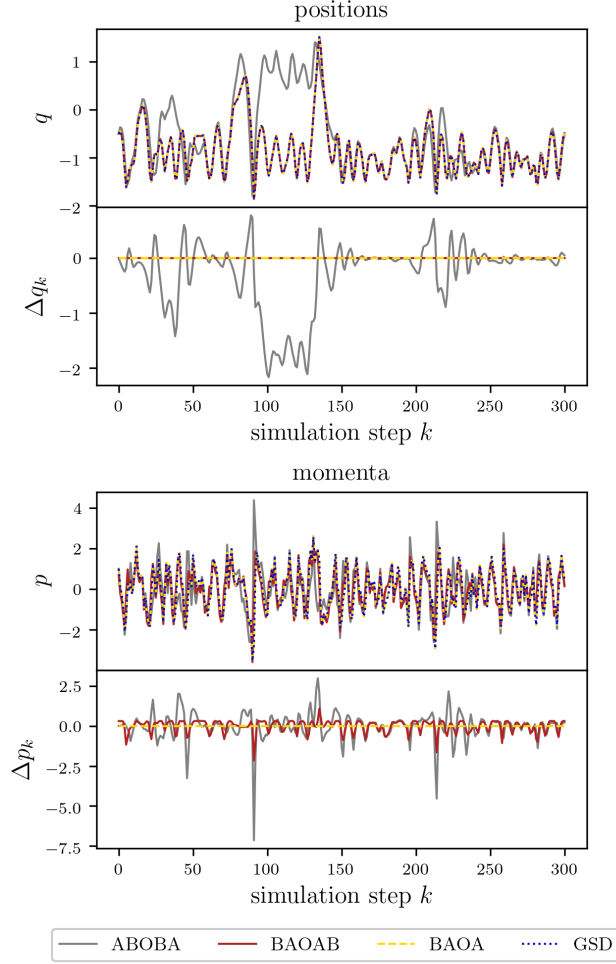


FIG. 1. Example trajectories in 1D potential with timestep  $\Delta t = 0.25$ . **Upper panel:** Position trajectories and deviations from GSD trajectory  $\Delta q_k^I = q_k^{\text{GSD}} - q_k^I$ . **Lower panel:** Momentum trajectories and deviations from GSD trajectory  $\Delta p_k^I = p_k^{\text{GSD}} - p_k^I$ . The initial momentum of BAOAB was shifted according to eq. 11.

Fig. 1 shows the position trajectories and the momentum trajectories, as well as the deviations from the GSD trajectory:  $\Delta q_k^I = q_k^{\text{GSD}} - q_k^I$  and  $\Delta p_k^I = p_k^{\text{GSD}} - p_k^I$ . The position trajectories of GSD, BAOA and BAOAB are identical. Additionally, the momentum trajectories of GSD and BAOA are identical, whereas the BAOAB momenta deviate slightly. This confirms our result from sections IIB and IIC. The ABOBA trajectory deviates in both the positions and the momenta from the GSD/BAOA trajectory.

Note that for a small timestep, the differences between the trajectories of the four integrators are much smaller (SI Fig. 2). This is expected, because all four integrators are guaranteed

to converge to the true dynamics for  $\Delta t \rightarrow 0$ . SI Fig. 3 shows the BAOAB trajectory for  $\Delta t = 0.25$ , if the initial momentum is not adjusted.

## B. Numerical accuracy

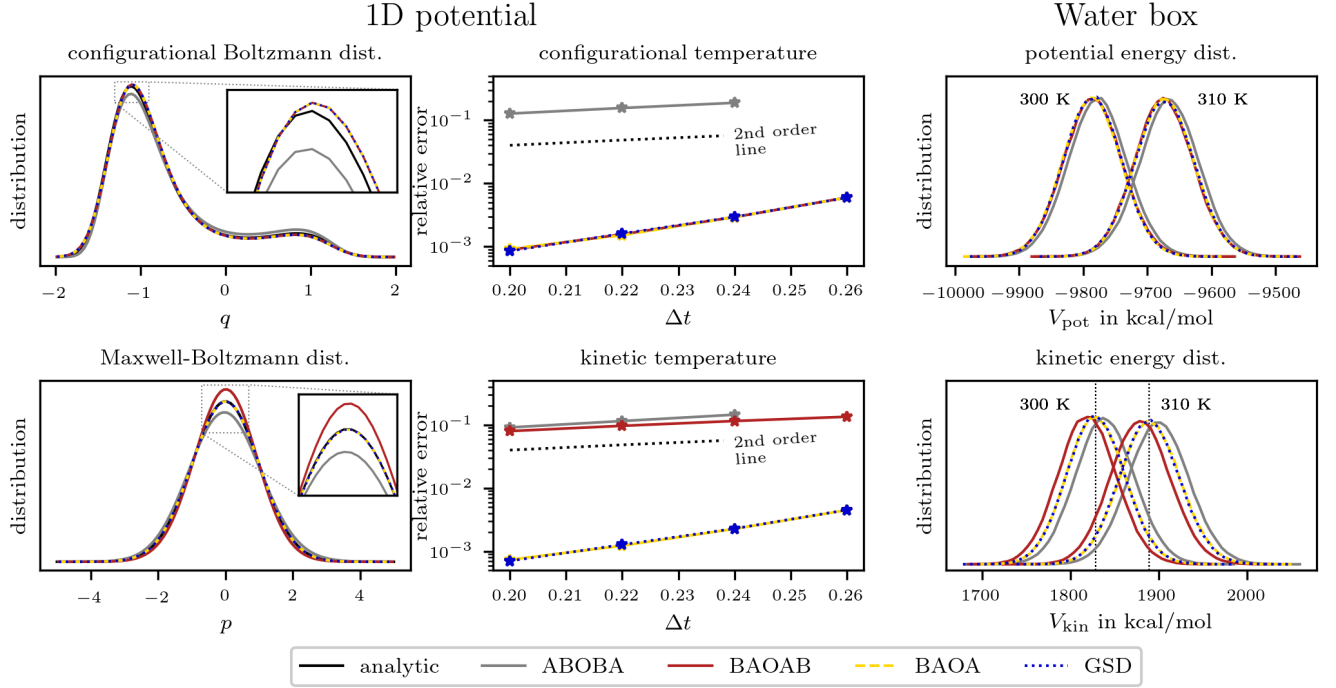


FIG. 2. Numerical accuracy. **left column:** Configurational Boltzmann distributions with the inset magnifying the region around the deepest well (top) and Maxwell-Boltzmann distributions with the inset magnifying the region around the mean momentum (bottom) for the 1D potential and  $\Delta t = 0.25$ . The analytic distributions are shown in black. **middle column:** Relative error in the average configurational temperature (top) and average kinetic temperature (bottom) for the 1D potential. The equation of the second order line is  $\varepsilon^{\text{2nd}} = \exp(\Delta t^2)$ . **right column:** Distributions of the total potential energy (top) and total kinetic energy (bottom) for TIP3P bulk water at near-ambient conditions and temperatures 300 K and 310 K. The vertical lines indicate the average kinetic energies expected by the equipartition theorem. Statistical uncertainties are smaller than the linewidth.

Next, we tested whether GSD and BAOA have the same numerical accuracy in the long-time limit. As model systems we use the one-dimensional tilted double-well potential from



section III A and a box of 1024 TIP3P water molecules<sup>37</sup>. (See SI section 2 for all simulation details.)

The left column in Fig. 2 tests how accurately ABOBA, BAOAB, GSD and BAOA reproduce the equilibrium distribution for the 1D potential in position and momentum space with a rather large timestep  $\Delta t = 0.25$ . GSD, BAOA and BAOAB generate the same configurational distribution. Their distribution agrees well with the analytical Boltzmann distribution (SI eq. 4), whereas the distribution generated by ABOBA deviates from the analytical solution. GSD and BAOA yield the same very accurate momentum distribution. (See SI eq. 5 for the analytical Maxwell-Boltzmann distribution.) BAOAB underestimates the variance in the momentum distribution leading to a higher peak at  $p = 0$ . Conversely, ABOBA overestimates the variance leading to a lower peak at  $p = 0$ . These results confirm that BAOAB, GSD and BAOA perform equally in configurational sampling while BAOAB differs from GSD and BAOA in momentum space.

The middle column in Fig. 2 reports the accuracy with which the integrators reproduce the target temperature in the 1D potential. We show the relative error  $\varepsilon(\Delta t) = (T_{\text{ref}} - T_{\text{approx}}(\Delta t))/T_{\text{ref}}$  as function of the timestep  $\Delta t$ . Smaller relative errors imply better accuracy. The relative error that is expected for an integrator with second order accuracy,  $\varepsilon^{\text{2nd}} = \exp(\Delta t^2)$ , is shown by the dotted line<sup>4</sup>.

The average temperature can either be computed as the configurational temperature  $T_{\text{conf}}$ , which is an average with respect to the configurational Boltzmann distribution, or as the kinetic temperature  $T_{\text{kin}}$ , which is an average with respect to the Maxwell-Boltzmann distribution (see SI section 2.A). In accordance with the observation that GSD/BAOA and BAOAB sample the same highly accurate configurational distribution, they also have the same low relative error in  $T_{\text{conf}}$ . In comparison, ABOBA yields less accurate configurational temperatures with more than 10 % discrepancy for all  $\Delta t$ . For  $T_{\text{kin}}$  the accuracy of GSD/BAOA differs from the accuracy of BAOAB. The relative error in the kinetic temperature sampled by GSD/BAOA is less than 1 % error for any given timestep. BAOAB yields less accurate kinetic temperatures with more than 10 % discrepancy in the  $\Delta t > 0.23$  regime, similar to the accuracy of ABOBA. This is line with the observation that GSD/BAOA samples the Maxwell-Boltzmann distribution very accurately.

The right column in Fig. 2 shows an accuracy test for a molecular system. Following Ref. 38 we determined the distributions of the total potential energy and total kinetic energy for bulk

TIP3P water<sup>37</sup> at near-ambient conditions and at two different temperatures, 300 K and 310 K, using a timestep of  $\Delta t = 2$  fs. (See SI section II.B for all simulation details.) We obtain an average potential energy of approximately -9780 kcal/mol at 300 K and -9670 kcal/mol at 310 K which is in good agreement with Ref. 38. The potential energy distributions of GSD/BAOA and BAOAB are visually indistinguishable for both temperatures, whereas the distribution of ABOBA is shifted to slightly higher potential energies. GSD and BAOA yield kinetic energy distributions whose means agree very well with the average kinetic energy that is expected from the equipartition theorem (dotted lines). (See SI, section 2.B.) The distribution of BAOAB is shifted to lower kinetic energies, which is in line with the underestimated variance of the Maxwell-Boltzmann distribution in the 1D-potential. Conversely, the distribution of ABOBA is slightly shifted to higher kinetic energies.

### C. Thermal rate constant

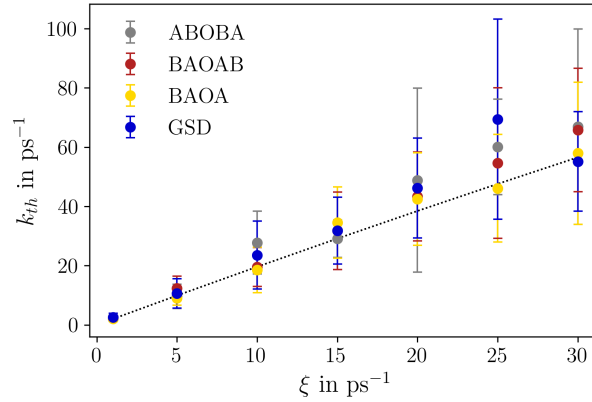


FIG. 3. Mean and standard deviation of the thermal rate constants  $k_{th}$  against the friction rate  $\xi$  for the ideal gas model. The black line represents the analytic solution for an ideal gas with Langevin friction (eq. 12).

An important property of a Langevin integrator is its ability to provide a single exponential decay in temperature towards the target temperature after a temperature change. The decay rate is called thermal relaxation rate  $k_{th}$  and can be adjusted via the friction rate  $\xi$ . Increasing  $\xi$  dampens the term related to the friction force  $\exp(-\xi\Delta t)p$  and increase the associated random force term  $\sqrt{(1 - \exp(-2\xi\Delta t))mk_B T \eta}$  in the O-step of the Langevin integrators (e.g. eq. 10c). At high values of  $\xi$ , fewer simulation steps are necessary to drive the

system towards the new target temperature, which corresponds to a high thermal relaxation rate  $k_{th}$ . At low values of  $\xi$ , the response to a change in temperature is slow. For an ideal gas with Langevin friction the relation between  $k_{th}$  and friction rate  $\xi$  is known analytically<sup>2</sup>

$$k_{th}^{\text{analytic}} = \frac{1 - \exp(-2\xi\Delta t)}{\Delta t}. \quad (12)$$

(dotted line in Fig. 3). Following Ref. 2, we determine the thermal relaxation rate  $k_{th}$  from simulations of an ideal gas in a cubic box for GSD, BAOA, BAOAB and ABOBA. All four algorithms show the expected first-order decay towards the target temperature. The thermal relaxation rates  $k_{th}$  are in good agreement with the analytic solution for all four integrators (Fig. 3). Their standard deviations increase with  $\xi$ , because at high friction rates the target temperature is reached within few timesteps ( $\mathcal{O}(100\text{ fs})$ ) which generates a numerical uncertainty in the fit of the decay curve.

#### IV. CONCLUSION

We have shown that GSD and BAOA are equivalent algorithms. Integrating eq. 1 by either integrator yields the same position and momentum trajectory (for a given random number sequence  $\boldsymbol{\eta}$ ). Consequently, GSD and BAOA have the same numerical accuracy for both, configurational and kinetic properties. Since BAOA and BAOAB sample the same positions<sup>3,36</sup> (for a given random number sequence  $\boldsymbol{\eta}$ ), we can now state that GSD, BAOA and BAOAB are equivalent configurational sampling algorithms. Our simulations confirm that GSD/BAOA achieves the same high numerical accuracy as BAOAB for configurational properties.

GSD/BAOA and BAOAB sample slightly different momentum trajectories. We find that GSD/BAOA is more accurate than BAOAB for kinetic properties. A similar finding is mentioned in the documentation of the MD package OpenMM<sup>39</sup>, where GSD/BAOA is called LF-Middle integrator (see eqs. 16 and 17 in Ref. 35). While this needs to be confirmed by a mathematical analysis of the convergence properties of GSD/BAOA and by numerical benchmarks with larger systems, our results suggest that GSD/BAOA samples configurations and momenta with excellent numerical accuracy.

Our results have several practical implications. Any analysis or benchmark of the configurational accuracy obtained for one of the three integrators equally applies to the other

two integrators. In particular, the stability of BAOAB with respect to large timesteps also applies to GSD/BAOA. Similarly, any extension of one of the integrators (e.g. incorporation of constraints<sup>35,40,41</sup> or multi-timestep algorithms<sup>30,31</sup>) can straightforwardly be transferred to the other two. The results also help in the development of path reweighting methods<sup>42–44</sup>, because equal Langevin integrators have equal path reweighting factors. Finally, with the combined experience gained with the GSD/BAOA and the BAOAB integrator, the MD community has a configurational sampling algorithm that has been tested and proven robust for system sizes and particle resolutions ranging from dissipative particle dynamics over coarse-grained and atomistic MD to path-integral MD.

## SUPPORTING INFORMATION

Detailed explanation of the computational methods and additional numerical results.

## ACKNOWLEDGEMENTS

We would like to thank Alexander H. de Vries, Nicu N. Goga and Benedict Leimkuhler for insightful discussions. This work was funded by Deutsche Forschungsgemeinschaft (DFG-German Research Foundation): project ID 235221301 (CRC 1114), project ID 431232613 (SFB 1449) and under Germany’s Excellence Strategy – EXC 2008/1 – 390540038.

## REFERENCES

- <sup>1</sup>P. H. Hünenberger, “Thermostat algorithms for molecular dynamics simulations,” in *Advanced Computer Simulation: Approaches for Soft Matter Sciences I* (Springer Berlin Heidelberg, 2005) pp. 105–149.
- <sup>2</sup>N. Goga, A. Rzepiela, A. De Vries, S. Marrink, and H. Berendsen, “Efficient algorithms for langevin and dpd dynamics,” *The Journal of Chemical Theory Computation* **8**, 3637–3649 (2012).
- <sup>3</sup>B. Leimkuhler and C. Matthews, “Rational Construction of Stochastic Numerical Methods for Molecular Sampling,” *Applied Mathematics Research eXpress* **48**, 278 (2012).
- <sup>4</sup>B. Leimkuhler and C. Matthews, “Robust and efficient configurational molecular sampling via Langevin dynamics,” *The Journal of Chemical Physics* **138**, 174102 (2013).

- <sup>5</sup>M. J. Abraham, T. Murtola, R. Schulz, S. Páll, J. C. Smith, B. Hess, and E. Lindahl, “Gromacs: High performance molecular simulations through multi-level parallelism from laptops to supercomputers,” *SoftwareX* **1**, 19–25 (2015).
- <sup>6</sup>B. A. Thurston, J. D. Tovar, and A. L. Ferguson, “Thermodynamics, morphology, and kinetics of early-stage self-assembly of  $\pi$ -conjugated oligopeptides,” *Molecular Simulation* **42**, 955–975 (2016).
- <sup>7</sup>M. Aldeghi, A. Heifetz, M. J. Bodkin, S. Knapp, and P. C. Biggin, “Predictions of ligand selectivity from absolute binding free energy calculations,” *Journal of the American Chemical Society* **139**, 946–957 (2017).
- <sup>8</sup>R. A. Mansbach, S. Chakraborty, K. Nguyen, D. C. Montefiori, B. Korber, and S. Gnanakaran, “The sars-cov-2 spike variant d614g favors an open conformational state,” *Science Advances* **7**, eabf3671 (2021).
- <sup>9</sup>S. J. Marrink and D. P. Tieleman, “Perspective on the martini model,” *Chemical Society Reviews* **42**, 6801–6822 (2013).
- <sup>10</sup>N. Goga, M. Melo, A. Rzepiela, A. De Vries, A. Hadar, S. Marrink, and H. Berendsen, “Benchmark of schemes for multiscale molecular dynamics simulations,” *Journal of Chemical Theory and Computation* **11**, 1389–1398 (2015).
- <sup>11</sup>G. Deichmann, M. Dallavalle, D. Rosenberger, and N. F. van der Vegt, “Phase equilibria modeling with systematically coarse-grained models—a comparative study on state point transferability,” *The Journal of Physical Chemistry B* **123**, 504–515 (2018).
- <sup>12</sup>W. Pezeshkian, M. König, T. A. Wassenaar, and S. J. Marrink, “Backmapping triangulated surfaces to coarse-grained membrane models,” *Nature Communications* **11**, 1–9 (2020).
- <sup>13</sup>A. G. Goicochea, M. B. Altamirano, J. Hernández, and E. Pérez, “The role of the dissipative and random forces in the calculation of the pressure of simple fluids with dissipative particle dynamics,” *Computer Physics Communications* **188**, 76–81 (2015).
- <sup>14</sup>S. Moga, G. Dragoi, A. Hadar, and N. Goga, “A parallelization scheme for new dpd-b thermostats,” *Journal of Atomic and Molecular Physics* **2013** (2013).
- <sup>15</sup>J. Schneider, J. Hamaekers, S. T. Chill, S. Smidstrup, J. Bulin, R. Thesen, A. Blom, and K. Stokbro, “Atk-forcefield: a new generation molecular dynamics software package,” *Modelling and Simulation in Materials Science and Engineering* **25**, 085007 (2017).
- <sup>16</sup>H. Jung, K.-i. Okazaki, and G. Hummer, “Transition path sampling of rare events by shooting from the top,” *The Journal of Chemical Physics* **147**, 152716 (2017).

- <sup>17</sup>A. Moga, I. Marin, N. Goga, A. Hadar, D. Geroge, and K. Oluwatoyin, “Improved openmm algorithms for cuda and opencl using new stochastic dynamics and the berendsen thermostat,” in *2015 6th International Conference on Computing, Communication and Networking Technologies (ICCCNT)* (IEEE, 2015) pp. 1–6.
- <sup>18</sup>D. Madeo, G. Bevilacqua, V. Biancalana, Y. Dancheva, and C. Mocenni, “A physical model for the characterization of magnetic hydrogels subject to external magnetic fields,” *Journal of Magnetism and Magnetic Materials* **493**, 165674 (2020).
- <sup>19</sup>“OpenMMTools Github,” <https://github.com/choderalab/openmmtools> (accessed: 07.02.2022).
- <sup>20</sup>J. Fass, D. A. Sivak, G. E. Crooks, K. A. Beauchamp, B. Leimkuhler, and J. D. Chodera, “Quantifying Configuration-Sampling Error in Langevin Simulations of Complex Molecular Systems,” *Entropy* **20**, 318 (2018).
- <sup>21</sup>P. Eastman, J. Swails, J. D. Chodera, R. T. McGibbon, Y. Zhao, K. A. Beauchamp, L.-P. Wang, A. C. Simmonett, M. P. Harrigan, C. D. Stern, R. P. Wiewiora, B. R. Brooks, and V. S. Pande, “Openmm 7: Rapid development of high performance algorithms for molecular dynamics,” *PLOS Computational Biology* **13**, 1 (2017).
- <sup>22</sup>Z. F. Brotzakis and P. G. Bolhuis, “Approximating free energy and committor landscapes in standard transition path sampling using virtual interface exchange,” *The Journal of Chemical Physics* **151**, 174111 (2019).
- <sup>23</sup>T. N. Starr, N. Czudnochowski, Z. Liu, F. Zatta, Y.-J. Park, A. Addetia, D. Pinto, M. Beltramello, P. Hernandez, A. J. Greaney, *et al.*, “Sars-cov-2 rbd antibodies that maximize breadth and resistance to escape,” *Nature* **597**, 97–102 (2021).
- <sup>24</sup>D. A. Sivak, J. D. Chodera, and G. E. Crooks, “Using nonequilibrium fluctuation theorems to understand and correct errors in equilibrium and nonequilibrium simulations of discrete langevin dynamics,” *Physical Review X* **3**, 011007 (2013).
- <sup>25</sup>A. D. Baczewski and S. D. Bond, “Numerical integration of the extended variable generalized langevin equation with a positive prony representable memory kernel,” *The Journal of Chemical Physics* **139**, 044107 (2013).
- <sup>26</sup>T. Plé, S. Huppert, F. Finocchi, P. Depondt, and S. Bonella, “Sampling the thermal wigner density via a generalized langevin dynamics,” *The Journal of Chemical Physics* **151**, 114114 (2019).

- <sup>27</sup>M. H. Duong and X. Shang, “Accurate and robust splitting methods for the generalized langevin equation with a positive prony series memory kernel,” arXiv preprint arXiv:2109.07879 (2021).
- <sup>28</sup>J. Liu, D. Li, and X. Liu, “A simple and accurate algorithm for path integral molecular dynamics with the langevin thermostat,” The Journal of Chemical Physics **145**, 024103 (2016).
- <sup>29</sup>N. Lopanitsyna, C. B. Mahmoud, and M. Ceriotti, “Finite-temperature materials modeling from the quantum nuclei to the hot electron regime,” Physical Review Materials **5**, 043802 (2021).
- <sup>30</sup>B. Leimkuhler, D. T. Margul, and M. E. Tuckerman, “Stochastic, resonance-free multiple time-step algorithm for molecular dynamics with very large time steps,” Molecular Physics **111**, 3579–3594 (2013).
- <sup>31</sup>L. Lagardère, F. Aviat, and J.-P. Piquemal, “Pushing the limits of multiple-time-step strategies for polarizable point dipole molecular dynamics,” The journal of Physical Chemistry Letters **10**, 2593–2599 (2019).
- <sup>32</sup>D. A. Sivak, J. D. Chodera, and G. E. Crooks, “Time step rescaling recovers continuous-time dynamical properties for discrete-time langevin integration of nonequilibrium systems,” The Journal of Physical Chemistry B **118**, 6466–6474 (2014).
- <sup>33</sup>B. Leimkuhler and C. Matthews, *Molecular Dynamics*. (Springer, 2016).
- <sup>34</sup>N. Bou-Rabee and H. Owhadi, “Long-run accuracy of variational integrators in the stochastic context,” SIAM Journal on Numerical Analysis **48**, 278–297 (2010).
- <sup>35</sup>Z. Zhang, X. Liu, K. Yan, M. E. Tuckerman, and J. Liu, “Unified efficient thermostat scheme for the canonical ensemble with holonomic or isokinetic constraints via molecular dynamics,” The Journal of Physical Chemistry A **123**, 6056–6079 (2019).
- <sup>36</sup>Z. Song and Z. Tan, “On irreversible metropolis sampling related to langevin dynamics,” arXiv preprint arXiv:2106.03012 (2021).
- <sup>37</sup>W. L. Jorgensen, J. Chandrasekhar, J. D. Madura, R. W. Impey, and M. L. Klein, “Comparison of simple potential functions for simulating liquid water,” The Journal of Chemical Physics **79**, 926–935 (1983).
- <sup>38</sup>E. Rosta, N.-V. Buchete, and G. Hummer, “Thermostat artifacts in replica exchange molecular dynamics simulations,” Journal of Chemical Theory and Computation **5**, 1393–1399 (2009).

- <sup>39</sup>“Documentation of the openmm python api: Langevinmiddleintegrator,” <http://docs.openmm.org/development/api-python/generated/openmm.openmm.LangevinMiddleIntegrator.html> (2015 (accessed: 30.03.2022)).
- <sup>40</sup>E. J. F. Peters, N. Goga, and H. J. Berendsen, “Stochastic dynamics with correct sampling for constrained systems,” *Journal of Chemical Theory and Computation* **10**, 4208–4220 (2014).
- <sup>41</sup>B. Leimkuhler and C. Matthews, “Efficient molecular dynamics using geodesic integration and solvent–solute splitting,” *Proceedings of the Royal Society A: Mathematical, Physical and Engineering Sciences* **472**, 20160138 (2016).
- <sup>42</sup>L. Donati, C. Hartmann, and B. G. Keller, “Girsanov reweighting for path ensembles and markov state models,” *The Journal of Chemical Physics* **146**, 244112 (2017).
- <sup>43</sup>L. Donati and B. G. Keller, “Girsanov reweighting for metadynamics simulations,” *The Journal of Chemical Physics* **149**, 072335 (2018).
- <sup>44</sup>S. Kieninger and B. G. Keller, “Path probability ratios for langevin dynamics—exact and approximate,” *The Journal of Chemical Physics* **154**, 094102 (2021).